Мезомасштабна камера згоряння є частиною малопотужного електрогенератора. Функція мезомасштабної камери згоряння полягає в перетворенні вуглеводня в теплову енергію в результаті реакції згоряння. Підтримання стійкості полум'я в мезомасштабній камері згоряння є важким через її міліметровий розмір.

Метою даного дослідження є визначення продуктивності і розпізнавання явищ мезомасштабних камер згоряння, що мають теплові рециркулятори з нержавіючої сталі. Це дослідження призначене для перевірки особливостей згоряння рідкого та газового палива в мезокамерах згоряння, що використовують тепловий рециркулятор. Тепловий циркулятор складається з труби з нержавіючої сталі з внутрішнім діаметром 3,5 мм. Спостережуваними параметрами були межі займистості, розподіл температури і візуалізація полум'я.

Підтверджено, що тепловий рециркулятор з нержавіючої сталі може використовуватися для підігріву і випаровування рідкого палива в мезомасштабній камері згоряння. Полум'я рідкого палива може стабілізуватися при коефіцієнті надлишку палива від 0,9 до 1,25 і приблизно до 900 градусів Цельсія. Таким чином, розробка рекомендується для малопотужного рідкопаливного генератора. Відзначено, що при занадто близькому розташуванні теплового рециркулятора до полум'я, відбувається надмірне охолодження полум'я, в результаті чого полум'я гасне. Мезокамера згоряння, яка не має теплового рециркулятора і призначена тільки для газового палива, здатна стабілізувати полум'я при коефіцієнті надлишку палива 0,7–1,5. Також підтверджено, що неточний вибір матеріалу теплового рециркулятора може привести до зниження стійкості полум'я. Важливо відзначити, що при виході газового палива з накопичувальної труби відбувається розширення та зниження температури, що може вплинути на межі займистості

Ключові слова: мікрокамера згоряння, займистість, рециркуляція тепла, рідке паливо, малопотужний генератор

UDC 536.3
DOI: 10.15587/1729-4061.2019.155347

THE USE OF HEAT CIRCULATOR FOR FLAMMABILITY IN MESOSCALE COMBUSTOR

A. F. H. Soegiharto
Lecturer
University of Muhammadiyah Malang
Jalan Raya Tlogomas, 246,
Malang, Indonesia, 65144
PhD student**
E-mail: achmadfauzan@umm.ac.id
I. N. G. Wardana
PhD, Professor*
E-mail: wardana@ub.ac.id
L. Yuliati
Doctor of Technical Sciences,
Associate Professor*
E-mail: lilis_y@ub.ac.id
M. N. Sasongko
Doctor of Technical Sciences,
Associate Professor*
E-mail: megasasongko@ub.ac.id
*Department of Mechanical Engineering**
**Universitas Brawijaya
Jalan. Mayjend Haryono, 167,
Malang, Indonesia, 65145

1. Introduction

The electric appliance is now increasingly widely used such as: types of portable electronic equipment, wireless equipment, space vehicles, security equipment and the military, as well as climate monitoring controllers. The electrical equipment such as cellular phones, notebook computers, GPS (global positioning systems), laptops, tablet computers, shavers, robots, unmanned aircrafts, radio communications, mini radars, micro pumps, micro motors, micro-robots, microturbines, etc. are the examples of the electric appliance. The equipment requires power supplies as conventional batteries. Conventional batteries as power suppliers have limitations, namely low energy density, relatively short lifetime, and hazardous waste. Conventional batteries also have problems with raw materials that are difficult to develop, because almost all potential ingredients have been used. This then leads to the development of micro-scale power generator technology or portable power generation technology [1].

Micropower generators are basically composed of two main parts, namely a) micro/mesoscale combustor and b) modules of energy conversion from thermal to electric. Micro/mesoscale combustors with stable combustion are very important parts in the micropower generator, which functions to convert the chemical energy of hydrocarbon fuel into heat energy through combustion [1–5]. It is difficult to maintain the stable flame inside of a micro/mesoscale combustor due to its millimetre-scale size.

The very small size of the combustion chamber produces a large surface-area-to-volume ratio, which results in a high rate of heat loss. The high rate of heat loss leads to flame cooling and causes flame instable and extinguished. The very small size of the combustion chamber also causes a short residence time of fuel and oxidants, which then causes an incomplete combustion reaction, and finally causes flame instability. All of these are the focus of research of micro/mesocombustor [4–25]. These problems produce various dynamics of flame behavior in the micro/mesoscale combustor. Therefore, it is very important to develop a micro/mesoscale

combustor with a wide operational flame stability range for power generation devices.

2. Literature review and problem statement

Various strategies and methods have been carried out by researchers to stabilize the flame in the micro/mesoscale combustor or increase the stability of the flame. Aspects studied about the microcombustor are as follows: combustion using porous media [21, 26–29], combustion using a catalyst [18, 30–33], combustion using a flame holder [9, 34–38], combustion utilizing thermal circulation. Combustion with thermal circulation itself consists of two kinds, first namely thermal circulation accompanied by gas circulation [2, 10, 39–43], included the swiss-roll type combustor [2, 43–46]. The second one is combustion by thermal circulation without gas circulation [14, 47] where heat is circulated to upstream for unburn gas preheating.

Gas fuel is widely used for investigating flame properties in micro/mesoscale combustors, due to its lightness compared to liquid fuels [8–10, 16, 20, 48–54].

But once the application on the micropower generator, the use of gas fuel is impractical due to the problem of safety and storage in a pressure-resistant tube. On the other hand, the weakness of liquid fuel for applications on the micropower generator is the difficult stabilization of the flame.

Even getting a stable combustion of liquid fuel in a micro/mesoscale combustor is a lot more problematic since there are transient phases of atomisation, evaporation, and mixing with an oxidant in a narrow combustion chamber. The preheating of liquid fuel requires an additional section or additional components or additional device or specific design [1, 14, 22, 23, 55].

Liquid fuel combustion in a mesoscale combustor has been successfully conducted through heat recirculation for reactant preheating. The reactant and product flows are created in such a way that there is a heat transfer from a combustion product to a reactant. The type of mesoscale combustor used is the Swiss-roll one [25].

Liquid fuel combustion in a narrow-tubed mesoscale combustor has also been successfully conducted with the support of electrospray device for atomisation and evaporation. The flame was successfully stabilised in a quartz-tubed mesoscale combustor that was put near or stuck to the inserted mesh. The mesh functioned as a flame holder, a droplet collector, to prolong the droplet's residence time, to preheat, and to vaporise the droplet through heat circulation [22, 23]. Further investigation of combustion on a quartz tube micro/mesoscale combustor with electrospray and the addition of an electrode ring has been carried out. The fuel used is ethanol without mixture. The results show that combustion efficiency can reach a maximum value of 90.5 % [15].

The combustion of hexane was successfully stabilised in a quartz-tubed mesoscale combustor without electrospray by using an inserted mesh as the flame holder and a copper heat recirculator. The heat recirculator wall comprised an annular chamber that covered up the main channel of the mesoscale combustor. There were five 0.5 mm-in-diameter holes functioned to distribute the vapour from the annulus chamber to the combustion chamber. What should be noted from the research is the use of copper as an essential component of the meso-combustor. Even though copper has high conductivity, it is easily deformed at high temperature [14]. Since it is easily deformed at high temperature, copper is rarely used as combustor material. A five-holed wall is more difficult to deploy than a four-holed one.

Based on the problems, the meso-combustor was redesigned by using a stainless-steel recirculator. To simplify the process, the number of holes was reduced from five to four.

3. The aim and objectives of the study

The aim of the research is to investigate the influence of the heat recirculator on the characteristics and behavior of the flame, related to the application of the micro/mesoscale combustor in the micropower generator.

To achieve this aim, the following objectives are accomplished:

– study on flame extinguishing by too high heat circulation;

– study on flame behavior related to the design of heat recirculator or micro/mesoscale combustor, by observing flammability limits, flame visualization, and temperature distribution;

– study on flame visualization due to the mixing of fuel and oxidant;

– study to recommend the design of heat recirculator or micro/meso-combustor to be applied to micropower generators.

4. Materials and methods

The mesoscale combustor used in this research is shown in Fig. 1, 2. This research used the 3.5 mm-in-diameter quartz-tubed mesoscale combustor with a line of 1 mm and an eight-holed plate of the flame holder as shown in Fig. 3.

The meso-combustor comprises four main parts, i. e.:

1) stainless-steel heat recirculator with annulus channel on its wall;

2) output section;

3) 3 mm stainless-steel insertion section;

4) a flame holder where the combustion occurs nearby.

In the previous research, the meso-combustor type A was used, where the flame holder was placed between the circulation section and the stainless-steel insertion section as shown in Fig. 2. In the following research, the meso-combustor type B was used. Fig. 3 shows the meso-combustor type C made by quartz glasses with flame folder insertion. Meanwhile, Fig. 4 shows a flame holder.

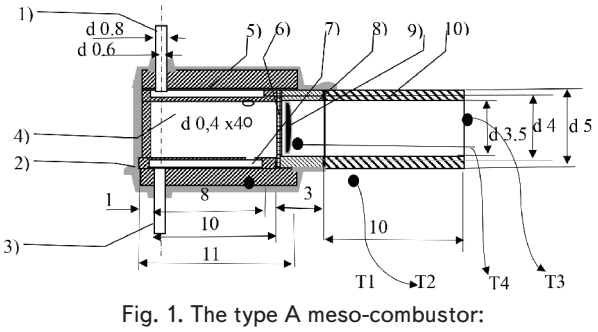

Fig. 1. The type A meso-combustor:
1 — fuel inlet, 2 — ceramic adhesive, 3 — air inlet, 4 — annulus channel, 5 — heat recirculator, 6 — flame holder, 7 — holes, 8 — the stainless steel insertion section, 9 — flame, outlet section

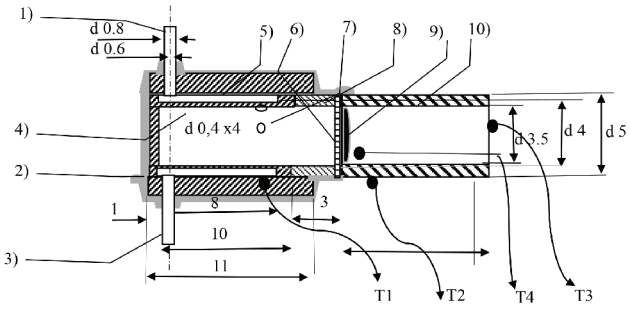

Fig. 2. The type B meso-combustor:
1 — fuel inlet, 2 — ceramic adhesive, 3 — air inlet, 4 — annulus channel, 5 — heat recirculator, 6 — flame holder, 7 — holes, 8 — the stainless steel insertion section, 9 — flame, Outlet section

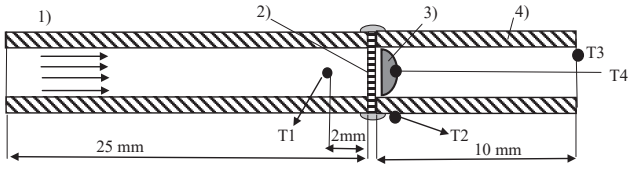

Fig. 3. The type C meso-combustor:
1 — quartz glass, 2 — flame holder, 3 — flame, 4 — quartz glass outlet section

Fig. 4. The flame holder

The meso-combustor was assembled on the research installation as shown in Fig. 5. The combustions on the type A and type B meso-combustor were alternately observed in Fig. 5 research installation.

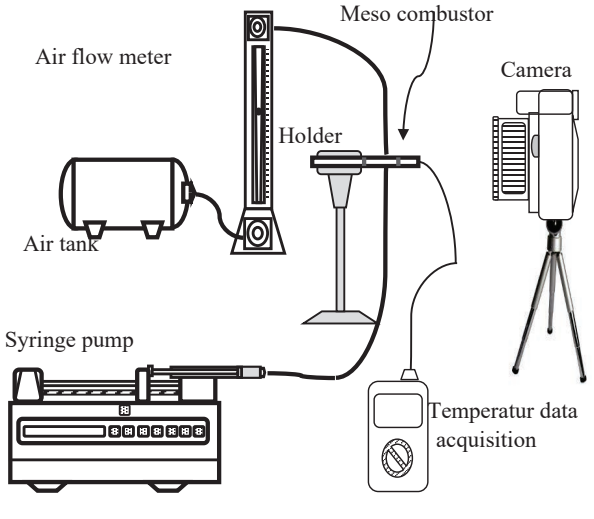

Fig. 5. The research installation with liquid fuel

The fuel used was hexane (C_6H_{10}) injected into the combustion chamber using a syringe pump. The syringe pump had the infusion rates from 0.73 μL/hr (1 mL syringe) to 2.100 μL/hr (60 mL syringe), NE 1000, New Era. The air was supplied from the air tank to the air inlet combustor, and the discharge was controlled by a flow meter (Koflock R 1250, with a measuring interval of 50–500 mL/minute, inlet pressure 0.1 MPa, and outlet pressure 0 MPa). The fuel and air were supplied to the combustor. An external heater was used for fuel preheating and evaporation. A torch was used to ignite a fire on the combustor's outlet. After the fire was ignited near the flame holder, the external heater was shut down. The fire remained burning due to heat recirculation from the flame to the fuel and the air through the flame holder, the stainless-steel insertion section, and the heat recirculator. The flame visualisation was documented by a macro-lens Nikon D5200 digital camera. A type K thermocouple with 0.1 mm in diameter connected to a data logger was used to measure the temperature.

The third experiment was conducted with the experimental installation as shown in Fig. 6. The butane was supplied from a butane tank, through a flowmeter (Koflock R 1250, with a measuring interval of 2–20 mL/minute, inlet pressure 0.1 MPa, and outlet pressure 0 MPa) to inlet 1 of the mesoscale combustor. The air from the air flow meter was distributed to inlet 2 of the mesoscale combustor.

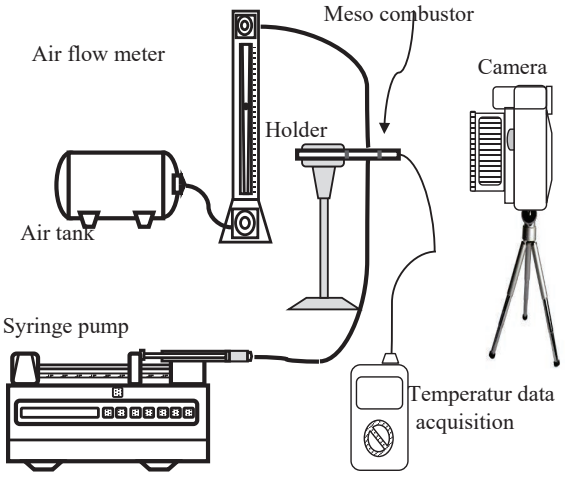

Fig. 6. The research installation for non-premix flame with gas fuel

The fourth experiment was conducted with the experimental installation as shown in Fig. 7.

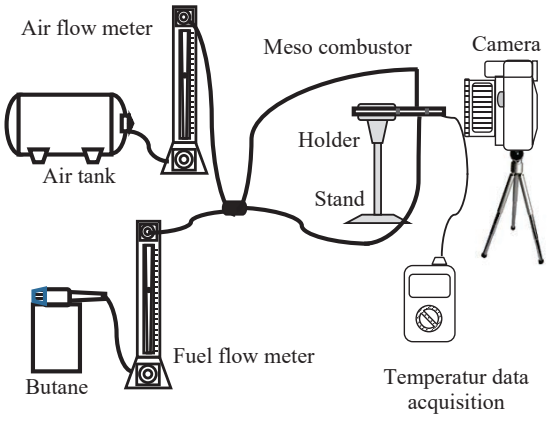

Fig. 7. The research installation for premix flame with gas fuel

The air was supplied from the air tank through the air flow meter, mixed with butane from the butane source tank through the fuel flow meter. The premix of butane-air was distributed to the inlet 1 and inlet 2 of the mesoscale combustor.

The fifth experiment was conducted with the experimental installation as shown in Fig. 8.

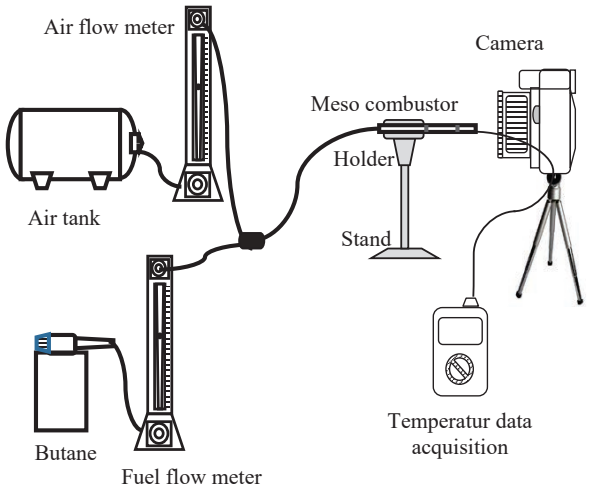

Fig. 8. The research installation by using the type C meso-combustor

The air was supplied from the air tank through the air flow meter, mixed with butane from the butane source tank through the fuel flow meter. The premix of butane and air was distributed to the type C mesoscale combustor.

All of the experiments were conducted on various compositions of fuel-air premix. The results are presented in the graphic of flame stability, the graphic of temperature, and the flame visualisation.

5. Experiment results

5. 1. Flame extinguishing by too high heat circulation

The initial experiment was conducted to obtain a combustion with a stable flame in the type A meso-combustor. At first, a fire was ignited outside the combustor, then the air and fuel discharges were set for a flashback to let the fire propagate into the combustor and remain stable there near the flame holder. When the fire contacted the flame holder, it died down and eventually went out. Once contacted the flame holder, it only lasted for 12 seconds, died down, and then went out in the next second, as shown in Fig. 9.

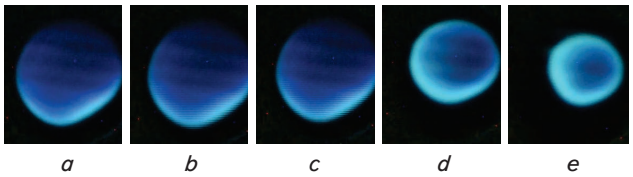

a *b* *c* *d* *e*

Fig. 9. The visualisation of flame burning and burnout: *a* — 4th second; *b* — 6th second; *c* — 8th second; *d* — 10th second; *e* — 12th second

Fig. 9 the visualization of flame burning and burnout of the first experiment. Hexane is supplied to the type A meso-combustor, where the recirculator segment coincides with the downstream of the flame holder. The flame is ignited from the downstream meso-combustor. Then the flame turns moving towards the flame holder. Momentary flame sticks to the flame holder, then shrinks and extinguished. The flame shrinkage is served every two seconds.

5. 2. Flame behavior related to the design of heat recirculator or micro/mesoscale combustor

The improvement of the type A meso-combustor is the type B meso-combustor, as shown in Fig. 2.

Fig. 10 the stability limits of hexane on the type B meso-combustor compared to the previous research. Hexane is supplied to the type B meso-combustor, where the recirculator section is separated by a 3 mm stainless steel segment from the flame holder. The flame is ignited from the downstream meso-combustor. The flame then turns moving towards the flame holder. The flame then attaches to the flame holder, then stabilizes. The observations of burning visualisation are shown in Fig. 11–13. The correlation between the temperature and the flow velocity is presented in Fig. 14, 15. The graphic of temperature on U=15 cm/s is presented in Fig. 16.

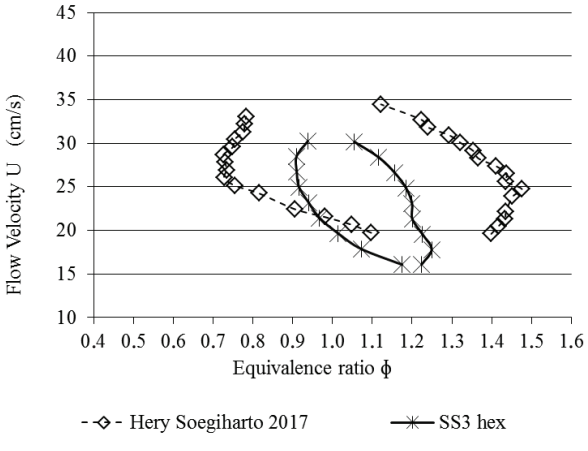

Fig. 10. The stability limits of hexane on the type B meso-combustor compared to the previous research (Hery Soegiharto, 2017)

The flame stability of two types of mesoscale combustor is shown in Fig. 10. The observations of burning visualisation are shown in Fig. 11–13. Fig. 11, *a* is the burning hexane visualisation in the type B meso-combustor and Fig. 11, *b* is the burning butane visualisation in the type B meso-combustor.

The correlation between the temperature and the flow velocity is presented in Fig. 14, 15. The graphic of temperature on U=15 cm/s is presented in Fig. 16.

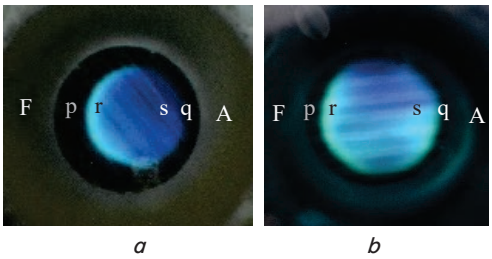

a *b*

Fig. 11. The flame visualisation in the type B meso-combustor: *a* — Hexane; *b* — Butane

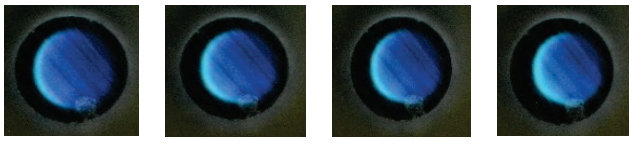

a *b* *c* *d*

Fig. 12. The flame visualisation of hexane at 20 cm/second reactant flow velocity: *a* – ϕ=0.9; *b* – ϕ=1.0; *c* – ϕ=1.1

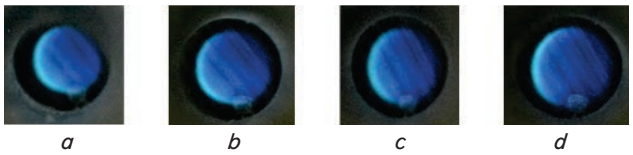

a *b* *c* *d*

Fig. 13. The flame visualisation of hexane in ϕ=0 equivalence ratio: *a* – *U*=17.69 cm/s; *b* – *U*=19.46 cm/s; *c* – *U*=21.23 cm/s; *d* – *U*=22.97 cm/s

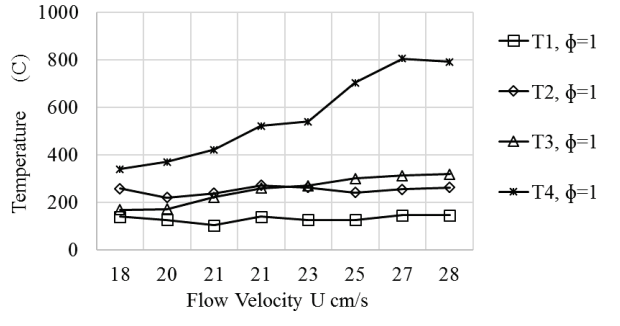

Fig. 14. The temperature hexane combustion at Equivalence Ratio ϕ=1

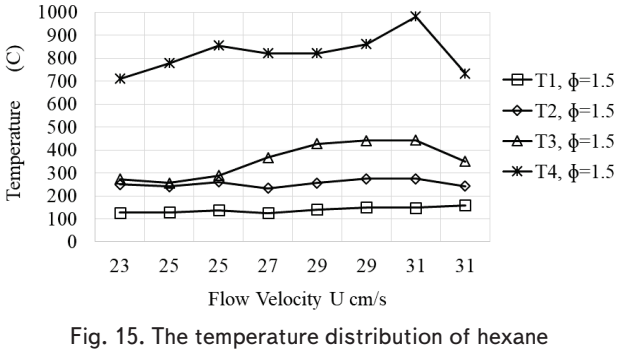

Fig. 15. The temperature distribution of hexane combustion at ϕ=1.5

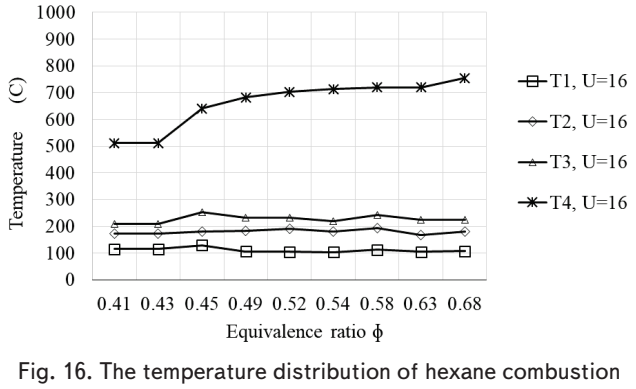

Fig. 16. The temperature distribution of hexane combustion at Flow Velocity *U*=16 cm/s

5. 3. Flame behavior due to the mixing of fuel and oxidant

The third experiment is combustion of non premix butane gas fuel by using the type B meso-combustor. The purpose of this experiment was to determine whether the tendency of dark light colors on flame occurred in combustion of hexane liquid fuels and also in combustion of butane gas fuel. The butane was supplied from a butane tank, through the flow-meter to inlet 1 of the mesoscale combustor. The air from the air flow meter was supplied to inlet 2 of the mesoscale combustor. The flame is ignited from the downstream of the meso-combustor. The flame then turns moving towards the flame holder. The flame then attaches to the flame holder, then stabilizes. The observations of burning visualisation are shown in Fig. 17. Temperature distribution is presented in Fig. 19, 20.

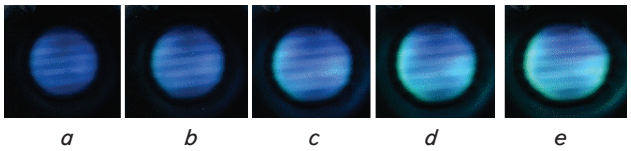

a *b* *c* *d* *e*

Fig. 17. Non-Premix Butane at flow velocity *U*=35 cm/s: *a* – ϕ=1.25; *b* – ϕ=1.33; *c* – ϕ=1.45; *d* – ϕ=1.55; *e* – ϕ=1.65

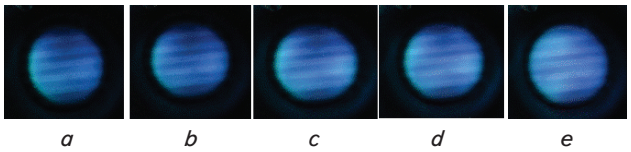

a *b* *c* *d* *e*

Fig. 18. Non Premix Butane at equivalence ratio ϕ=1.4: *a* – *U*=27 cm/s; *b* – *U*=31 cm/s; *c* – *U*=35 cm/s; *d* – *U*=37 cm/s; *e* – *U*=41 cm/s

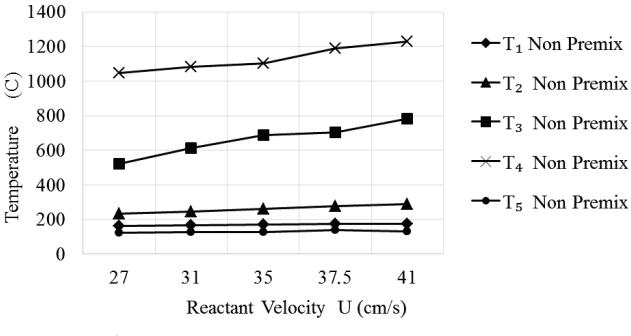

Fig. 19. The temperature distribution of non-premix Butane at ϕ=1.4

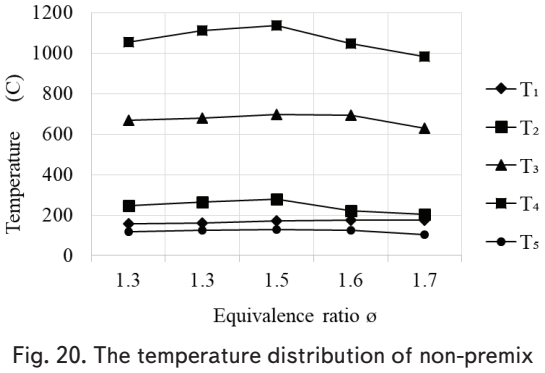

Fig. 20. The temperature distribution of non-premix Butane at *U*=35 cm/s

The fourth experiment is combustion of premix butane gas fuel by using the type B meso-combustor. The air was supplied from the air tank through the air flow meter, mixed

with butane from the butane source tank through the fuel flow meter. The premix of butane-air was distributed to the inlet 1 and inlet 2 of the mesoscale combustor. The flame is ignited from the downstream of the meso-combustor. The flame then turns moving towards the flame holder. The flame then attaches to the flame holder, then stabilizes. The observations of burning visualisation are shown in Fig. 21. Comparison of temperature distribution of premix and non premix butane is presented in Fig. 23, 24.

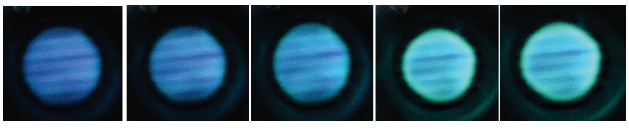

Fig. 21. Premix Butane at flow velocity U=35 cm/s: *a* – ϕ=1.25; *b* – ϕ=1.33; *c* – ϕ=1.45; *d* – ϕ=1.55; *e* – ϕ=1.65

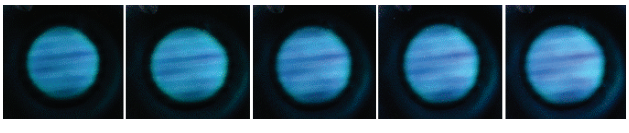

Fig. 22. Premix Butane at equivalence ratio ϕ=1.4: *a* – U=27 cm/s; *b* – U=31 cm/s; *c* – U=35 cm/s; *d* – U=37.5 cm/s; *e* – U=41 cm/s

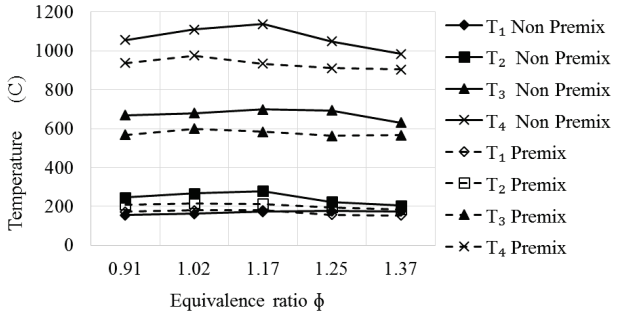

Fig. 23. Premix and non-premix temperature vs equivalence ratio

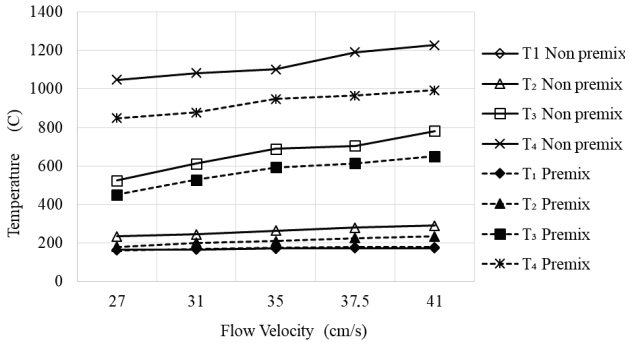

Fig. 24. The temperature distribution of Type B Butane

Fig. 25, express flammability limits of hexane and butane inside of any type of meso-combustor. The Fig. 25, *a* curve is flammability limits of hexane by using the type B meso-combustor. The Fig. 25, *b* curve is flammability limits of non premix butane by using the type B meso-combustor. The Fig. 25, *c* curve is flammability limits of premix butane by using the type B meso-combustor. The Fig. 25, *d* curve is flammability limits of premix butane by using the type C meso-combustor.

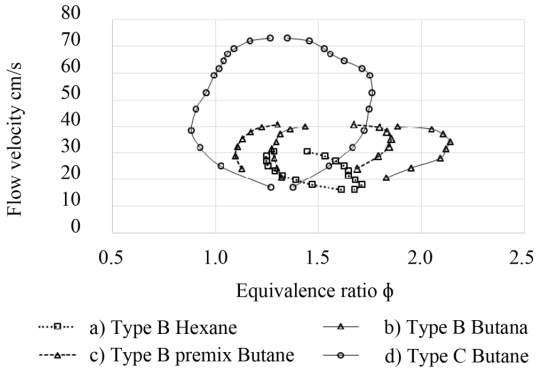

Fig. 25. Flammability limits of hexane and butane inside of any type of meso-combustor

6. Discussion of the research results regarding the role of heat recirculator for flame stabiles in mesoscale combustor

The fuel used in the experiment of Fig. 9 was hexane. In a liquid phase, hexane requires intense heat to evaporate before combusted. The four 0.4 mm-in-diameter holes were assumed too small to distribute the fuel vapour from the annulus channel to the combustion chamber. This led to the slow combustion, reduction of heat production, fuel accretion in the annulus channel, and cooling of the heat recirculator. The close proximity of the flame holder to the annulus channel where hexane was injected caused the flame in the flame holder cooled down.

In the type A meso-combustor, the flame was stabilised in a 3-mm stainless-steel section that attached to the flame holder. Some produced heat was conducted to the stainless-steel heat exchanger section (the upstream part) and to the quartz section (the downstream part). The upstream part got more heat than the downstream one. The heat conducted to the upstream part was used for preheating and vaporisation. If the amount of conducted heat is too small, the flame will be less stable. On the other hand, an exorbitant amount of heat will cool down the flame and will disturb the flame stability. Therefore, the heat distribution to the upstream part was slightly adjusted by reducing the heat absorption by the wall in the burning area.

The improvement of the type A meso-combustor is the type B meso-combustor, as shown in Fig. 2. The flame holder was set apart from the annulus channel and was put to a more downstream position, between the stainless insertion section and the quartz outlet section. This way, the flame heat was not directly cooled by the fuel. The way is equal to the mesh insertion as a droplet collector in the quartz-tubed meso-combustor for stabilizing the burning of liquid fuel. In that experiment, the insertion of mesh droplet collector has prevented the blackout by liquid fuel droplets [22].

In the type B meso-combustor, the burning of hexane has successfully stabilised near or on the flame holder. The heat was distributed or was absorbed by the quartz wall. The absorbance was not as much as through stainless steel of the type A meso-combustor. The heat was conducted to

the upstream and the downstream parts. The heat was distributed to the upstream part through the insertion of 3-mm stainless-steel section and was forwarded to the annulus heat exchanger. The insertion of a 3 mm stainless-steel section prevented the burnout by fuel in the annulus chamber.

The flame stability of two types of mesoscale combustor is shown in Fig. 10. The observations of burning visualisation are shown in Fig. 11–13. Fig. 11, *a* is the burning hexane visualisation in the type B meso-combustor and Fig. 11, *b* is the burning butane visualisation in the type B meso-combustor. The fuel was injected from the *F* direction, while the air was injected from the A direction. The bright blue colour (*r*) was produced by the burning of a rich mixture. The brighter the flame, the higher the equivalence ratio is (Fig. 12). Meanwhile, the dark blue colour (*s*) was produced by the burning of a lean mixture. The aperture without flame (*p*) was caused by the over lean reactant mixture that exceeded its flammability limit and thus known as the flammability limit distance. The aperture without flame (*q*) that divided the lean mixture from the wall was the result of the blackout by the wall and known as the quenching distance. The same phenomenon happened on the meso-combustor with copper recirculation section [14].

The mechanism of colour gradation is illustrated in Fig. 26. On the heat recirculator, there was an annulus wall covering the main channel of the mesoscale combustor. The air was injected into the annulus chamber on the opposite side of the fuel inlet. In the annulus channel, along with its position towards the downstream part, the air mixed with the fuel. However, there were not enough space and time for homogenous mixing. The fuel inlet side produced a rich mixture with high equivalence ratio. Meanwhile, the air inlet side produced a lean mixture with low equivalence ratio.

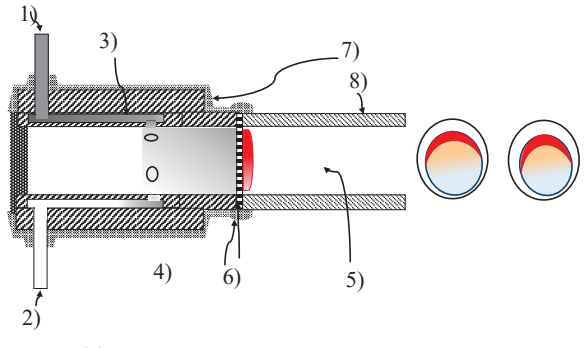

Fig. 26. An illustration of reactant flow and mixing: (1) Fuel inlet, (2) Air inlet, (3) Annulus channel, (4) Stainless steel heat reciculator, (5) Flame, (6) Flame holder, (7) Ceramic adhesive, (8) outlet

The correlation between the temperature and the flow velocity is presented in Fig. 14, 15. The temperature was observed on four points, i. e. the heat recirculator (T1), the wall near the flame (T2), the side of the exhaust gas outlet (T3), and the flame (T4). The measuring of flame temperature (T4) was conducted by inserting the thermocouple from the downstream part of the meso-combustor. Meanwhile, the temperature distribution of the hexane combustion is shown in Fig. 14 for the equivalence ratio $\phi=1$. The temperature in the annulus chamber (T1) was approximately 113 °C to 140 °C with the average of 127 °C. This indicated that the fuel in the measuring point has become super-heated steam after passing through evaporation at its boiling point (69 °C). The air-fuel mixture entered the main chamber of the meso-combustor and passed through the flame holder and ended in the flame area. The average temperature of the wall around the flame (T2) was 246 °C. The average temperature of the exhaust gas was 244 °C. Meanwhile, the average flame temperature was 590 °C. At the low flow velocity, the temperature of the exhaust gas (T3) tended to be low, even lower than the temperature of the combustor's wall (T2). The more increase in flow velocity, the higher the flame temperature (T4) became. At a high speed of reactant, the flame temperature reached 800 °C.

The amount of combustion heat carried away with the flow of exhaust gas was also increased and thus arose the temperature of exhaust gas (T3). The temperature of the exhaust gas became higher than the temperature of the wall around the flame (T2). This indicated that more heat was wasted along with the exhaust gas than those circulated to the upstream part.

At the equivalence ratio $\phi=1.5$, the fuel mixture is richer than the stoichiometric condition ($\phi=1$). The curve of temperature correlation is presented in Fig. 15. The flow velocity increase was accompanied by the rising of flame temperature (T4) and exhaust gas temperature (T3). The higher the flow velocity, the greater the number of inserted and combusted reactant became. On the other hand, the higher the flow velocity, the shorter the reactants' residence time in the meso-combustor became. As a consequence, the fuel did not fully combust and then wasted along with the combustion gas. In this condition, the addition of the reactant mixture would damp down the flame. As shown in Fig. 15, the temperature drops when the flow velocity is high.

The graphic of temperature on $U=15$ cm/s is presented in Fig. 16. There was a tendency that high equivalence ratio f contributed to more fuel combustion, more energy production, and higher flame temperature.

Fig. 11, *b* is the visualisation of butane combustion in the type B mesoscale combustor. The fuel was injected from the left direction, while the air was injected from the right. The bright blue colour was apparent near the fuel side (left). However, both the bright and the dark blue colours became dimmer than those shown in the flame visualisation of hexane combustion. The aperture without flame around the butane flame had relatively the same thickness. However, at a high equivalence ratio, the bright blue colour of butane at the fuel side (left) side became more apparent (Fig. 17) and the aperture without flame at the fuel side (left) side became a little thicker. This happened since the air-butane mixture is more homogenous than the air-liquid hexane mixture.

Fig. 17 also shows the thickening of the aperture without a flame that occurred at a high equivalence ratio. The increase in the equivalence ratio means the addition of butane into the meso-combustor. The addition cooled the wall down and prevented the burning of reactant around the wall and thus wasted away. When this happened, the temperature went down as shown in Fig. 20. The waste of a small amount of fuel indicates the high consumption of fuel or the increasing equivalence ratio.

Fig. 18 shows the visualisation of butane flame in the type B meso-combustor where butane and air were injected from different channels. The flame seemed brighter at the high flow velocity. The flame diameter did not indicate a significant change. The aperture without flame also did not show any change in thickness. At a constant equivalence ratio and a higher flow velocity, the addition of butane and

the addition of air coincided proportionally. Meanwhile, the addition of flow velocity means the addition of reactant, hence the addition of combustion heat. As shown in Fig. 19, the higher the temperature, the greater the flow velocity obtained.

When butane is released from a high-pressure tank, an expansion and temperature drop occurred. This is assumed as the cause of temperature drop and the cooling of the wall in the type B meso-combustor and the increasing equivalence ratio.

To figure out whether the bright-dark colour gradation is indeed caused by the channel system and fuel insertion or not, an experiment using the premix butane was conducted. The measured air and butane were mixed and injected into the annulus chamber of the meso-combustor. The visualisations of premix butane flame are shown in Fig. 21, 22. The flame formed a perfect circle and there was no thickening of the aperture without a flame on one of the sides. This occurred at both the constant flow velocity and the constant equivalence ratio. The flame circle showed an equal spread of bright and dark colours. This showed that the colour gradation at one side was indeed caused by the channel system and the fuel insertion in the meso-combustor used in the experiment.

Fig. 21 shows the visualisation of premix butane combustion at the flow velocity U=35 cm/s. The aperture without flame thickened along with the increasing equivalence ratio. Since it was a premix combustion, the thickening of the aperture without flame was not caused by the over lean reactant. Instead, it was caused by the cooling of butane when it expanded. The aperture without flame caused the waste of a small amount of fuel, decreasing combustion heat, and temperature drop, as shown in Fig. 24.

Fig. 22 shows the visualisation of premix butane combustion at the flow equivalence ratio ϕ=1.4. The flame diameter of the premix butane combustion at both the low and high flow velocity remained the same. The aperture without flame had the same thickness at both the high and the low flow velocity. The flame became a little brighter along with the increasing flow velocity. The addition of flow velocity means the proportional addition of reactant (both air and butane). This was followed by the addition of combustion heat indicated by temperature rise, as shown in Fig. 27.

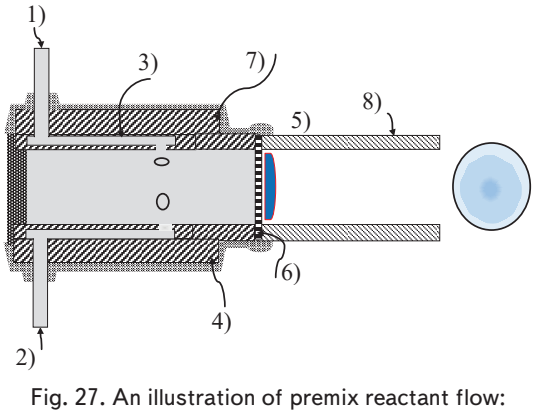

Fig. 27. An illustration of premix reactant flow:
(1) Fuel inlet, (2) Air inlet, (3) Annulus channel, (4) Stainless steel heat reciculator, (5) Flame, (6) Flame holder, (7) Ceramic adhesive, (8) outlet

Fig. 27 shows the illustration of the flow of butane-air premix that was inserted through the second hole of the inlet channel. Since the beginning, the air and the fuel have already mixed. The mixture entered the main chamber of the meso-combustor, i.e. the burning area with homogenous-coloured flame.

The flame stability of hexane combustion in the type B meso-combustor is shown in the curve (*a*) in Fig. 10. The area of stable flame existed between both of the curves (*a*). In the area where the equivalence ratio is lower than the minimum flammability limits of hexane, the flame could not be stabilised, or in other words, blew out. This also happened in the area with a higher equivalence ratio. The flame stability of hexane in the type B meso-combustor was narrower than the flame stability of the type B meso-combustor that was made from copper (*e*). The narrowing of the flammability limits of hexane flame in the type B meso-combustor was affected by the thermal conductivity and the thermal diffusivity. The thermal conductivity and the thermal diffusivity of stainless steel are lower than of copper.

Fig. 25 is the graphic of flammability limits of hexane and butane combustion in the type B meso-combustor. Curve (*b*) is the flammability limits of butane combustion in the type B meso-combustor, where the fuel and the air are injected into the recirculation section separately. Curve (*c*) is the flammability limits of butane premix combustion in the type B meso-combustor. Meanwhile, curve (*d*) is the flammability limits of butane combustion in the type C meso-combustor.

The curve of flammability limits (*a*) is the narrowest one among the other curves in Fig. 25. Curve (*a*) is the flame of liquid hexane. The application of the meso-combustor is for the micropower electric generator. The more practical fuel for this is the liquid fuel, regarding its packaging and safety. However, in a meso-combustor, the liquid fuel is harder to burn than the gas one. This is because the liquid fuel combustion should initially pass through the evaporation phase. In this research, the evaporation of hexane occurred in the recirculation section of the type B meso-combustor.

The flame of non-premix butane in the type B meso-combustor has successfully stabilized with the curve of flammability limits (*a*) that was wider than the curve of flammability limits (*b*). The butane, which is in the form of gas, did not require additional heat to evaporate and thus did not absorb the flame's heat. This led to a wider range of flammability limits.

The flame of non-premix butane (curve (*b*)) occurred in a higher equivalence ratio and a wider range than that occurred in the flame of premix butane (curve (*c*)). It means that the non-premix butane combustion in the type B meso-combustor consumed more fuel than the premix butane combustion and thus resulted in a higher temperature as shown in Fig. 23, 24.

Fig. 25 is the visualization of the flame of diffusion butane (the premix of butane and hexane). The use of premix butane resulted in a more homogeneous mix. The homogeneity of the mix will affect the perfection of the butane combustion reaction in the mesoscale combustor. One of its indications is the absence of brighter and darker side of the flame.

The butane combustion in the type C meso-combustor produced better flame stability than the heat recirculator. It is seen in curve (*d*) that has a wider range than (*b*) and (*c*). In conclusion, the stainless-steel heat recirculator in the type B meso-combustor caused more heat loss, the use of heat recirculator was actually meant to increase the heat recirculation from the flame to the reactant at the upstream part. The heat recirculation was meant to preheat the reactant so that the reactant could gain sufficient energy to produce a flame. In turn, the recirculator was expected to be able to

increase the flammability limits. The inexact heat recirculator could increase the heat loss and thus could end with constriction of flammability limits.

As a part of the micropower electric generator, the mesoscale combustor was installed along with the other device such as thermophotovoltaic material to produce electricity. The type B meso-combustor having recirculation section with the annulus chamber inside its wall was proven useful to stabilize the flame of liquid hexane. The liquid fuel produced a narrow flame stability, which means it is harder to maintain the flame. However, it has better quality in terms of packaging simplicity, energy density, and safety. Thus, the type B meso-combustor is suitable as an alternative to be used in the liquid-fuel based micropower electric generator.

For the combustion of non-premix gas butane, the type B meso-combustor provided a wider range of flame stability and a higher temperature than when it was used for the combustion of premix butane. Therefore, it is better to use the non-premix butane when the type B meso-combustor is installed in the micropower electric generator. The wider range of flame stability can be obtained by using the type C meso-combustor with gas fuel. This type of combustor cannot be used with liquid fuel.

7. Conclusions

1. The type B meso-combustor having recirculation section with the annulus chamber inside its wall was proven useful to stabilise the flame of liquid hexane. As a part of the micropower electric generator, the mesoscale combustor should be installed along with the other device such as thermophotovoltaic material to produce electricity.

2. It is confirmed that the stainless steel heat recirculator, is useful for liquid fuel preheating and evaporating inside of the mesoscale combustor. The flame of liquid fuels can be stabilized at an equivalence ratio of 0.9 to 1.25, and up to about 900 centigrade Celsius. Thus recommend for liquid fuel micropower generator. It is noted that when the heat recirculator is too close to the flame, excessive flame cooling occurs and causes the flame extinguished. The meso-combustor, which has no heat recirculator, and designed for gas fuel only, can stabilize flame at an equivalence ratio of 0.7 to 1.5. It is also confirmed that the inaccurate selection of material of thermal recirculator risks reducing the flame stability.

It is important to note that when the gas fuel exits the storage tube, there is an expansion and a decrease in temperature which can affect flammability limits.

3. For the combustion of non-premix gas butane, the type B meso-combustor provided a wider range of flame stability and a higher temperature than when it was used for the combustion of premix butane. Therefore, it is better to use the non-premix butane when the type B meso-combustor is installed in the micropower electric generator. The wider range of flame stability can be obtained by using the type C meso-combustor with gas fuel. This type of combustor cannot be used with liquid fuel.

References

1. Development of micro power generators – A review / Chou S. K., Yang W. M., Chua K. J., Li J., Zhang K. L. // Applied Energy. 2011. Vol. 88, Issue 1. P. 1–16. doi: https://doi.org/10.1016/j.apenergy.2010.07.010
2. Fan A., Zhang H., Wan J. Numerical investigation on flame blow-off limit of a novel microscale Swiss-roll combustor with a bluff-body // Energy. 2017. Vol. 123. P. 252–259. doi: https://doi.org/10.1016/j.energy.2017.02.003
3. Wierzbicki T. A., Lee I. C., Gupta A. K. Performance of synthetic jet fuels in a meso-scale heat recirculating combustor // Applied Energy. 2014. Vol. 118. P. 41–47. doi: https://doi.org/10.1016/j.apenergy.2013.12.021
4. Higuchi K., Nakano T., Takahashi S. Development of portable power unit with catalytic micro-combustor // Journal of Physics: Conference Series. 2018. Vol. 1052. P. 012058. doi: https://doi.org/10.1088/1742-6596/1052/1/012058
5. Field synergy analysis of the micro-cylindrical combustor with a step / E J., Zuo W., Liu H., Peng Q. // Applied Thermal Engineering. 2016. Vol. 93. P. 83–89. doi: https://doi.org/10.1016/j.applthermaleng.2015.09.028
6. Compact design of planar stepped micro combustor for portable thermoelectric power generation / Aravind B., Raghuram G. K. S., Kishore V. R., Kumar S. // Energy Conversion and Management. 2018. Vol. 156. P. 224–234. doi: https://doi.org/10.1016/j.enconman.2017.11.021
7. Aravind B., Khandelwal B., Kumar S. Experimental investigations on a new high intensity dual microcombustor based thermoelectric micropower generator // Applied Energy. 2018. Vol. 228. P. 1173–1181. doi: https://doi.org/10.1016/j.apenergy.2018.07.022
8. Effect of the cavity depth on the combustion efficiency of lean H2/air flames in a micro combustor with dual cavities / Yang W., Xiang Y., Fan A., Yao H. // International Journal of Hydrogen Energy. 2017. Vol. 42, Issue 20. P. 14312–14320. doi: https://doi.org/10.1016/j.ijhydene.2017.03.235
9. Wan J., Zhao H. Dynamics of premixed CH4/air flames in a micro combustor with a plate flame holder and preheating channels // Energy. 2017. Vol. 139. P. 366–379. doi: https://doi.org/10.1016/j.energy.2017.08.002
10. Experimental investigation on combustion characteristics of premixed propane/air in a micro-planar heat recirculation combustor / Tang A., Cai T., Deng J., Xu Y., Pan J. // Energy Conversion and Management. 2017. Vol. 152. P. 65–71. doi: https://doi.org/10.1016/j.enconman.2017.09.011
11. Nakamura Y., Gao J., Matsuoka T. Progress in small-scale combustion // Journal of Thermal Science and Technology. 2017. Vol. 12, Issue 1. P. JTST0001–JTST0001. doi: https://doi.org/10.1299/jtst.2017jtst0001
12. A review of combustion-driven thermoelectric (TE) and thermophotovoltaic (TPV) power systems / Mustafa K. F., Abdullah S., Abdullah M. Z., Sopian K. // Renewable and Sustainable Energy Reviews. 2017. Vol. 71. P. 572–584. doi: https://doi.org/10.1016/j.rser.2016.12.085

13. A heat-recirculating combustor with multiple injectors for thermophotovoltaic power conversion / Kim T. Y., Kim H. K., Ku J. W., Kwon O. C. // Applied Energy. 2017. Vol. 193. P. 174–181. doi: https://doi.org/10.1016/j.apenergy.2017.02.040
14. The Role of Liquid Fuels Channel Configuration on the Combustion inside Cylindrical Mesoscale Combustor / Hery Soegihar-to A. F., Wardana I. N. G., Yuliati L., Nursasongko M. // Journal of Combustion. 2017. Vol. 2017. P. 1–9. doi: https://doi.org/10.1155/2017/3679679
15. Experimental study on electro-spraying and combustion characteristics in meso-scale combustors / Gan Y., Tong Y., Ju Y., Zhang X., Li H., Chen X. // Energy Conversion and Management. 2017. Vol. 131. P. 10–17. doi: https://doi.org/10.1016/j.enconman.2016.11.015
16. Alipoor A., Saidi M. H. Numerical study of hydrogen-air combustion characteristics in a novel micro-thermophotovoltaic power generator // Applied Energy. 2017. Vol. 199. P. 382–399. doi: https://doi.org/10.1016/j.apenergy.2017.05.027
17. Investigation of energy conversion and flame stability in a curved micro-combustor for thermo-photovoltaic (TPV) applications / Akhtar S., Khan M. N., Kurnia J. C., Shamim T. // Applied Energy. 2017. Vol. 192. P. 134–145. doi: https://doi.org/10.1016/j.apenergy.2017.01.097
18. Experiments on n -heptane combustion with two types of catalyst layouts / Yang W., Zhou M., Deng C., Huang T., Zhou J., Wang Z. et. al. // Applied Thermal Engineering. 2016. Vol. 100. P. 325–332. doi: https://doi.org/10.1016/j.applthermaleng.2016.02.010
19. Fabrication and characterization of thermoelectric power generators with segmented legs synthesized by one-step spark plasma sintering / Li S., Pei J., Liu D., Bao L., Li J.-F., Wu H., Li L. // Energy. 2016. Vol. 113. P. 35–43. doi: https://doi.org/10.1016/j.energy.2016.07.034
20. Jiang D., Yang W., Tang A. Development of a high-temperature and high-uniformity micro planar combustor for thermophotovoltaics application // Energy Conversion and Management. 2015. Vol. 103. P. 359–365. doi: https://doi.org/10.1016/j.enconman.2015.06.083
21. Experimental study of n-heptane/air combustion in meso-scale burners with porous media / Li J., Huang J., Yan M., Zhao D., Zhao J., Wei Z., Wang N. // Experimental Thermal and Fluid Science. 2014. Vol. 52. P. 47–58. doi: https://doi.org/10.1016/j.expthermflusci.2013.08.021
22. Combustion of gaseous and liquid fuels in meso-scale tubes with wire mesh / Mikami M., Maeda Y., Matsui K., Seo T., Yuliati L. // Proceedings of the Combustion Institute. 2013. Vol. 34, Issue 2. P. 3387–3394. doi: https://doi.org/10.1016/j.proci.2012.05.064
23. Yuliati L., Seo T., Mikami M. Liquid-fuel combustion in a narrow tube using an electrospray technique // Combustion and Flame. 2012. Vol. 159, Issue 1. P. 462–464. doi: https://doi.org/10.1016/j.combustflame.2011.06.010
24. Experimental study on micro modular combustor for micro-thermophotovoltaic system application / Yang W. M., Jiang D. Y., Chou S. K., Chua K. J., Karthikeyan K., An H. // International Journal of Hydrogen Energy. 2012. Vol. 37, Issue 12. P. 9576–9583. doi: https://doi.org/10.1016/j.ijhydene.2012.03.129
25. Shirsat V., Gupta A. K. Performance characteristics of methanol and kerosene fuelled meso-scale heat-recirculating combustors // Applied Energy. 2011. Vol. 88, Issue 12. P. 5069–5082. doi: https://doi.org/10.1016/j.apenergy.2011.07.019
26. Effects of external heating on flame stability in a micro porous combustor fuelled with heptane / Chen X., Li J., Feng M., Wang N. // Combustion Science and Technology. 2019. Vol. 191, Issue 2. P. 311–324. doi: https://doi.org/10.1080/00102202.2018.1463220
27. Giovannoni V., Sharma R. N., Raine R. R. Premixed combustion of methane–air mixture stabilized over porous medium: A 2D numerical study // Chemical Engineering Science. 2016. Vol. 152. P. 591–605. doi: https://doi.org/10.1016/j.ces.2016.06.039
28. Dynamic behaviors of premixed hydrogen–air flames in a planar micro-combustor filled with porous medium / Li J., Wang Y., Shi J., Liu X. // Fuel. 2015. Vol. 145. P. 70–78. doi: https://doi.org/10.1016/j.fuel.2014.12.070
29. Coutinho J. E. A., de Lemos M. J. S. Laminar flow with combustion in inert porous media // International Communications in Heat and Mass Transfer. 2012. Vol. 39, Issue 7. P. 896–903. doi: https://doi.org/10.1016/j.icheatmasstransfer.2012.06.002
30. A study of methanol steam reforming on distributed catalyst bed / Wang G., Wang F., Li L., Zhang G. // International Journal of Hydrogen Energy. 2013. Vol. 38, Issue 25. P. 10788–10794. doi: https://doi.org/10.1016/j.ijhydene.2013.02.061
31. Bijjula K., Vlachos D. G. Catalytic ignition and autothermal combustion of JP-8 and its surrogates over a $Pt/\gamma\text{-}Al_2O_3$ catalyst // Proceedings of the Combustion Institute. 2011. Vol. 33, Issue 2. P. 1801–1807. doi: https://doi.org/10.1016/j.proci.2010.05.008
32. Enhancement of methane combustion in microchannels: Effects of catalyst segmentation and cavities / Li Y.-H., Chen G.-B., Hsu H.-W., Chao Y.-C. // Chemical Engineering Journal. 2010. Vol. 160, Issue 2. P. 715–722. doi: https://doi.org/10.1016/j.cej.2010.03.057
33. Lee M. J., Kim N. I. Experiment on the effect of Pt-catalyst on the characteristics of a small heat-regenerative CH_4 – air premixed combustor // Applied Energy. 2010. Vol. 87, Issue 11. P. 3409–3416. doi: https://doi.org/10.1016/j.apenergy.2010.04.033
34. Wan J., Zhao H. Thermal performance of solid walls in a mesoscale combustor with a plate flame holder and preheating channels // Energy. 2018. Vol. 157. P. 448–459. doi: https://doi.org/10.1016/j.energy.2018.05.189
35. Wan J., Shang C., Zhao H. Dynamics of methane/air premixed flame in a mesoscale diverging combustor with/without a cylindrical flame holder // Fuel. 2018. Vol. 232. P. 659–665. doi: https://doi.org/10.1016/j.fuel.2018.06.026
36. Wan J., Shang C., Zhao H. Anchoring mechanisms of methane/air premixed flame in a mesoscale diverging combustor with cylindrical flame holder // Fuel. 2018. Vol. 232. P. 591–599. doi: https://doi.org/10.1016/j.fuel.2018.06.027
37. Wan J., Fan A., Yao H. Effect of the length of a plate flame holder on flame blowout limit in a micro-combustor with preheating channels // Combustion and Flame. 2016. Vol. 170. P. 53–62. doi: https://doi.org/10.1016/j.combustflame.2016.05.015

38. Wan J., Fan A. Effect of solid material on the blow-off limit of CH_4/air flames in a micro combustor with a plate flame holder and preheating channels // Energy Conversion and Management. 2015. Vol. 101. P. 552–560. doi: https://doi.org/10.1016/j.enconman.2015.06.010
39. Effects of heat recirculation on combustion characteristics of n-heptane in micro combustors / Li J., Huang J., Chen X., Zhao D., Shi B., Wei Z., Wang N. // Applied Thermal Engineering. 2016. Vol. 109. P. 697–708. doi: https://doi.org/10.1016/j.applthermaleng.2016.08.085
40. Numerical study of the geometrical parameters on CH4/air premixed combustion in heat recirculation micro-combustor / Yan Y., Pan W., Zhang L., Tang W., Chen Y., Li L. // Fuel. 2015. Vol. 159. P. 45–51. doi: https://doi.org/10.1016/j.fuel.2015.06.069
41. Scale and material effects on flame characteristics in small heat recirculation combustors of a counter-current channel type / Lee M. J., Cho S. M., Choi B. I., Kim N. I. // Applied Thermal Engineering. 2010. Vol. 30, Issue 14-15. P. 2227–2235. doi: https://doi.org/10.1016/j.applthermaleng.2010.06.003
42. Effect of heat recirculation on the self-sustained catalytic combustion of propane/air mixtures in a quartz reactor / Scarpa A., Pirone R., Russo G., Vlachos D. G. // Combustion and Flame. 2009. Vol. 156, Issue 5. P. 947–953. doi: https://doi.org/10.1016/j.combustflame.2008.11.005
43. Chen W.-H., Cheng Y.-C., Hung C.-I. Transient reaction and exergy analysis of catalytic partial oxidation of methane in a Swiss-roll reactor for hydrogen production // International Journal of Hydrogen Energy. 2012. Vol. 37, Issue 8. P. 6608–6619. doi: https://doi.org/10.1016/j.ijhydene.2012.01.054
44. Zhong B.-J., Wang J.-H. Experimental study on premixed CH4/air mixture combustion in micro Swiss-roll combustors // Combustion and Flame. 2010. Vol. 157, Issue 12. P. 2222–2229. doi: https://doi.org/10.1016/j.combustflame.2010.07.014
45. Development and scale effects of small Swiss-roll combustors / Il Kim N., Aizumi S., Yokomori T., Kato S., Fujimori T., Maruta K. // Proceedings of the Combustion Institute. 2007. Vol. 31, Issue 2. P. 3243–3250. doi: https://doi.org/10.1016/j.proci.2006.08.077
46. Flame stabilization and emission of small Swiss-roll combustors as heaters / Kim N., Kato S., Kataoka T., Yokomori T., Maruyama S., Fujimori T., Maruta K. // Combustion and Flame. 2005. Vol. 141, Issue 3. P. 229–240. doi: https://doi.org/10.1016/j.combustflame.2005.01.006
47. Munir F. A., Mikami M. A numerical study of propane-air combustion in meso-scale tube combustors with concentric rings // Journal of Thermal Science and Technology. 2015. Vol. 10, Issue 1. P. JTST0008–JTST0008. doi: https://doi.org/10.1299/jtst.2015jtst0008
48. Development of micro-thermophotovoltaic power generator with heat recuperation / Yang W. M., Chua K. J., Pan J. F., Jiang D. Y., An H. // Energy Conversion and Management. 2014. Vol. 78. P. 81–87. doi: https://doi.org/10.1016/j.enconman.2013.10.040
49. Improvement of Combustion Stability in Narrow tubes with wire Mesh / Munir F. A., Hatakeda N., Seo T., Mikami M. // ISTP_Fudhail_Rev4_ISTP final. 2014.
50. Taywade U. W., Deshpande A. A., Kumar S. Thermal performance of a micro combustor with heat recirculation // Fuel Processing Technology. 2013. Vol. 109. P. 179–188. doi: https://doi.org/10.1016/j.fuproc.2012.11.002
51. Combustion characteristics of a small-scale combustor with a percolated platinum emitter tube for thermophotovoltaics / Li Y.-H., Chen G.-B., Cheng T.-S., Yeh Y.-L., Chao Y.-C. // Energy. 2013. Vol. 61. P. 150–157. doi: https://doi.org/10.1016/j.energy.2013.09.003
52. Jiang D., Yang W., Chua K. J. Entropy generation analysis of H2/air premixed flame in micro-combustors with heat recuperation // Chemical Engineering Science. 2013. Vol. 98. P. 265–272. doi: https://doi.org/10.1016/j.ces.2013.05.038
53. Deshpande A. A., Kumar S. On the formation of spinning flames and combustion completeness for premixed fuel – air mixtures in stepped tube microcombustors // Applied Thermal Engineering. 2013. Vol. 51, Issue 1-2. P. 91–101. doi: https://doi.org/10.1016/j.applthermaleng.2012.09.013
54. Flame propagation in a tube with wall quenching of radicals / Bai B., Chen Z., Zhang H., Chen S. // Combustion and Flame. 2013. Vol. 160, Issue 12. P. 2810–2819. doi: https://doi.org/10.1016/j.combustflame.2013.07.008
55. DuttaRoy R., Chakravarthy S. R., Sen A. K. Experimental investigation of flame propagation and stabilization in a meso-combustor with sudden expansion // Experimental Thermal and Fluid Science. 2018. Vol. 90. P. 299–309. doi: https://doi.org/10.1016/j.expthermflusci.2017.09.008